Friction
https://doi.org/10.1007/s40544-021-0559-4
ISSN 2223-7690
CN 10-1237/TH
RESEARCH ARTICLE

Long-term tribocorrosion resistance and failure tolerable of multilayer carbon-based coatings

Hao LI[1,2], Linlin LIU[1], Peng GUO[1,*] Lili SUN[1], Jing WEI[1], Yingrui LIU[1,2], Shuyu LI[1,2], Shuyuan WANG[1,2], Kwang-Ryeol LEE[1,3], Peiling KE[1,2], Aiying WANG[1,2,*]

[1] *Key Laboratory of Marine Materials and Related Technologies, Zhejiang Key Laboratory of Marine Materials and Protective Technologies, Ningbo Institute of Materials Technology and Engineering, Chinese Academy of Sciences, Ningbo 315201, China*

[2] *Center of Materials Science and Optoelectronics Engineering, University of Chinese Academy of Sciences, Beijing 100049, China*

[3] *Computational Science Center, Korea Institute of Science and Technology, Seoul 136-791, Republic of Korea*

Received: 08 February 2021 / Revised: 19 June 2021 / Accepted: 30 September 2021

Abstract: Current tribocorrosion research of metallic materials and their surface protective coatings mainly focuses on their short-term properties, with test time of 0.5–2.0 h and a sliding distance 50–500 m, which may significantly deviate from the practical long-term service condition and thus cause a catastrophe of marine equipments. In this study, three carbon-based multilayer coatings (Ti/DLC, TiC_x/DLC, and Ti–TiC_x/DLC) were deposited on S32750 substrates, and both short-term and long-term tribocorrosion behaviors were investigated. The experimental results indicate that the coatings substantially improve the tribocorrosion resistance of the S32750 stainless steel. During the short-term tribocorrosion test, TiC_x/DLC exhibited the best tribocorrosion resistance owing to its high hardness. During the long-term tribocorrosion test, however, Ti–TiC_x/DLC coating indicated the best anti-tribocorrosion performance owing to its excellent fracture toughness together with high hardness. Moreover, under 5 N, Ti–TiC_x/DLC can withstand a long-term test of more than 24 h. Additionally, under a higher load of 20 N, the Ti–TiC_x/DLC with a corresponding sliding distance of approximately 1,728 m maintained a low friction coefficient of approximately 0.06. However, the coating was completely worn out; this is attributable to the formation of tribocorrosion products consisting of graphitized carbon and nanocrystalline Fe_xO_y.

Keywords: DLC; multilayer structure; long-term tribocorrosion; failure tolerance

1 Introduction

Currently, the marine industry plays a progressively crucial role in global economic and social development. With the increasing development of marine sectors, the need for marine infrastructures and components with high durability and reliability is rapidly increasing [1]. In practice, however, conventional metallic components are subjected to harsh marine environments. Moreover, the exposure to ultraviolet radiation, the chloride-rich salty environment, frequent wet-dry cycles, high humidity, low temperature, and the presence of seawater could accelerate the degradation and failure of structural materials [2].

Application of a protective coating onto metal substrates is an economic and effective method for improving the anti-corrosion and anti-tribocorrosion properties of mechanical components [3–5], specifically for critical moving components used in marine engineering equipment. For instance, Wu et al. deposited a Cr–Si–C–N coating on a 316L stainless steel using unbalanced magnetron sputtering technology, which effectively improved the wear and corrosion resistance of the substrate in artificial seawater [3]. Liu et al.

* Corresponding authors: Peng GUO, E-mail: guopeng@nimte.ac.cn; Aiying WANG, E-mail: aywang@nimte.ac.cn

established that plasma-sprayed Al_2O_3 coating could decrease the pore resistance (R_{po}) and increase the charge transfer resistance (R_t) of Q235 steel during tribocorrosion [4].

Among the various types of protective coatings, diamond-like carbon (DLC), as a representative amorphous carbon film, has been widely employed in the triobocorrosion protection of metal materials because of its high hardness, low coefficient of friction, chemical stability, and biocompatibility [6–10]. For instance, Totolin et al. confirmed that the W-based DLC exhibited better tribocorrosion resistance compared to the untreated Ti6Al4V substrate, which was attributed to its improved frictional characteristics, low wear scar depth, and stable open circuit potential (OCP) [5]. By co-doping small amount of Cr/Cu elements into DLC matrix, Sun et al. found that the coating exhibited the combined good properties such as antifouling, corrosion resistance and low friction of coefficient [11]. Moreover, by using the designed multilayer structure, not only the improvement of elastic recovery and inhibition of crack propagation was obtained [12], the superior friction behavior was also achieved under both dry condition and boundary lubrications with various contact pressures [13, 14]. In particular, Zhang et al. compared the tribological behaviors of DLC films with monolayered and multilayered structure in dry conditions, in which the multilayered films significantly reduced the wear rate without deterioration of coefficient of friction (COF) [15]. Meanwhile, Bai et al. confirmed that the a-C multilayer films enhanced both the corrosion and wear resistance compared to those of the monolayer a-C film [16]. In addition, our previous simulation confirmed that using Ti layers benefited the formation of carbon roll structure and interfacial adhesion strength at lower temperature (T < 900 K), which played the stronger catalyzed effect on the graphitic transformation of amorphous carbon interface [12].

Notably, in aggressive aqueous environments, some carbon-based coatings can still have a low COF although they are substantially worn out [13, 14, 17, 18]. This can be attributed to the damage tolerance of the carbon-based coating, which helps in designing high-performance anti-tribocorrosion coatings. However, owing to a paucity of studies, the cause of the damage tolerance of the carbon-based coatings is still uncertain.

Although the protective coatings exhibited improved tribocorrosion properties, the usual tribocorrosion test time and sliding distance were approximately 0.5–2.0 h and 50–500 m, respectively, and the longest time and distance were not more than 6.0 h and 1,000 m, respectively, as shown in Fig. S1 in the Electronic Supplementary Material (ESM) [3–6, 19–28]. Owing to the complicated interaction between corrosive and mechanical damage, the long-term tribocorrosion properties and failure mechanism of the coatings can pose a challenge in, which is an urgent and challenging subject, maintaining the long-term reliability and durability of marine equipment [3–5, 29].

In this study, the carbon-based multilayer coatings were prepared on the S32750 stainless steel, and their short-term and long-term tribocorrosion behaviors in a 3.5 wt% NaCl solution were studied. In addition, the damage tolerance characteristics of the coatings in tribocorrosion were analyzed.

2 Experimental

2.1 Sample preparation

UNS S32750 super duplex stainless steel (SDSS) was selected as the substrate material for coating deposition. This is because it exhibits an excellent combination of corrosion resistance and mechanical properties, and it has been widely used in the offshore and marine industries dealing with tribocorrosion [30, 31]. The S32750 alloy sheet was purchased from Nippon Yakin Kogyo Co., Ltd. Kawasaki Plant. It has a nominal chemical composition (in wt%) of 0.020 C, 0.20 Si, 0.79 Mn, 0.026 P, 6.4 Ni, 25.8 Cr, 3.3 Mo, 0.09 Cu, 0.30 N, and Fe balance. After machining it into standardized specimens with a size of 18 mm × 18 mm × 3 mm, the S32750 substrates were sequentially ground using a series of SiC abrasive papers to 3,000 grit, and then finely polished to mirror finish with 0.3 μm chromic oxide slurry. In addition, a p-type (100) Si wafer was synchronously used as a substrate for the microstructure and mechanical characterization of the prepared coatings. Before the deposition of the coatings, all substrates were ultrasonicated with alcohol

(10 min) followed by deionized water (10 min), and finally dried through nitrogen gas blowing.

As shown in Fig. 1(a), the multilayered coatings were designed and prepared. Combining the multilayers with a top-layer thickening structure proved to be an effective strategy for achieving high-performance tribocorrosion properties for carbon-based coatings [27]. The Ti/DLC coating, having a Ti adhesion layer and a thickened DLC top layer, was composed of periodically stacked alternating Ti and DLC layers. For the TiC_x/DLC coating, TiC_x replaced the Ti interlayer because it made more great contribution to stress relaxation and interfacial adhesion enhancement [32, 33]. Furthermore, the Ti–TiC_x/DLC coating was specialized to minimize the interfacial mismatch by substituting Ti interlayer with the TiC_x–Ti–TiC_x sandwich layer.

As schematized in Fig. 1(b), the multilayered coatings were deposited using a hybrid system combining linear anode-layer ion source (LIS) and direct current magnetron sputtering (DCMS) techniques. To deposit the Ti and TiC_x interlayers in inert (Ar) and reactive (Ar/C_2H_2) atmospheres, respectively, high-purity titanium target (99.99%, dimensions of 400 mm × 100 mm × 7 mm) served as the magnetron cathode of the sputtering system. The substrates were mounted on a rotating substrate holder at a distance of approximately 15 cm from the sputtering target and the ion source. Prior to deposition, the deposition chamber was heated to 150 °C and then evacuated to a base vacuum of 2.0×10^{-5} Torr. To remove the undesirable oxide and improve the coating adhesion, the substrates were first cleaned and etched by introducing high-purity argon (99.999%) at a flow rate of 35 sccm into the ion source with an overall power of 300 W for 30 min, and a pulse negative bias voltage of –200 V was subsequently applied to the substrates. During deposition, a Ti (or TiC_x) adhesion layer was first sputter deposited from the Ti target with a target current of 3.0 A at an Ar flow rate of 50 sccm. For the TiC_x layer deposition, high-purity acetylene (99.999%) with a flow rate of 5 sccm was supplied as the reactive gas. After the deposition of the adhesion layer, a DLC layer was deposited using LIS with a C_2H_2 flow rate of 38 sccm and a direct current of 0.2 A. Thereafter, the Ti (or TiC_x, TiC_x–Ti–TiC_x) layer and the DLC layer were alternatively deposited via DCMS and LIS with a rotating substrate holder located at positions 1 and 2, respectively, as shown in Fig. 3(b). For the aforementioned coatings, five periods of stacking Ti/TiC_x/TiC_x–Ti–TiC_x and DLC layers were prepared. During the deposition process, a pulse negative bias voltage of –150 V was applied to the substrates. More details of sample preparation can be referred in our previous work [27, 34].

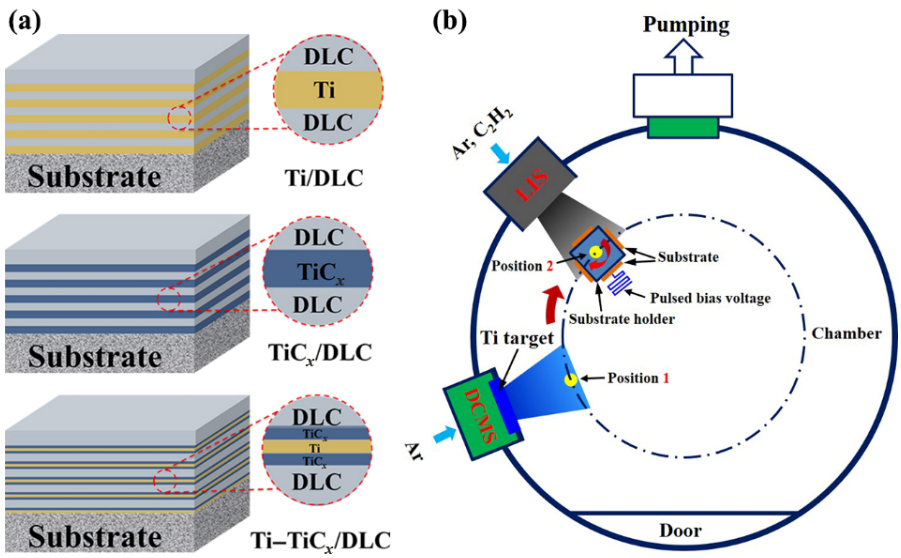

Fig. 1 (a) Schematic structural design of the carbon-based multilayer coatings; (b) schematic diagram of a hybrid LIS/DCMS deposition system.

2.2 Microstructural characterization

Scanning electron microscopy (SEM, Verios G4 UC, USA) was used to evaluate the surface morphology, cross-sectional microstructure, and thickness of the coatings. Atomic force microscopy (AFM, 3100v, Veeco, USA) was used to analyze the surface topography of the coatings, with a scanning probe microscope tapping mode set at a scanning frequency of 2.0 Hz. The root-mean-square roughness (Rq) of the coatings was calculated from 512 × 512 surface height data points obtained from a scan area of 5 μm × 5 μm. A confocal micro-Raman spectrometer (Renishaw inVia-reflex, UK) was used to characterize the bonding structure. All measurements were performed in air at room temperature with a wavelength of 532 nm. For the DLC coatings, Raman data can be fitted using a Gaussian line shape to show the disorder D, amorphous graphitic G peak positions, and the ratio of peak intensities (I_D/I_G). High-resolution transmission electron microscopy (TEM, Tecnai F20, USA) was performed to observe the microstructure of the coatings. TEM samples were prepared using a focused ion beam instrument (FIB, Carl Zeiss, Auriga, Germany), and a platinum layer was preliminarily deposited to protect the surface of the sample before FIB treatment.

2.3 Mechanical tests

The hardness and elastic modulus values were measured using a continuous load-controlled nano-indentator (MTS NANO200, USA). The diamond indenter was a Berkovich tip. The load was 10 mN, and 12 indents were used. To avoid the influence of the substrate, the maximum penetration was 20% of the coating thickness. Vickers indentation tests were performed on an automatic digital micro hardness tester (MVS-1000D1) with a normal load of 4.9 N to test the toughness of the coating.

2.4 Tribocorrosion investigations

The tribocorrosion tests were conducted in a 3.5 wt% NaCl solution, using a ball-on-disk reciprocating tribometer (Rtec, USA), which was connected with a three electrochemical cell (Mudulab). The system comprised an Al_2O_3 ceramic ball (1,800 HV, Φ 6 mm) as the counterpart, coatings as the working electrode, saturated calomel electrode (SCE) as the reference electrode, and a platinum plate as the counter electrode. All sliding tests were conducted under a sliding rate of 20 mm/s, a stroke length of 5 mm, and a normal load of 5 N, during which the OCP and COF were simultaneously recorded. The tests were performed after 1 h of sample immersion, once the potential of the samples was stabilized. In addition, it was empirically known that the corrosion resistance, surface activation and electrochemical repair ability of the coatings could be characterized based on the OCP evolution. Three replicates of each material were tested to ensure the reproducibility of the results. A surface profilometer (Alpha-Step IQ, USA) was employed after the tribocorrosion test to determine the volume and area of the worn track.

3 Results and discussion

3.1 Microstructure and composition

Figures 2(a)–2(c) display the surface topographies of the multilayered coatings. All the coatings showed a compact and fine surface without visible defects, and various cauliflower-like structures were observed. According to the AFM, the Rq of the Ti/DLC, TiC_x/DLC, and Ti–TiC_x/DLC were 19.4, 6.9, and 12.3 nm, respectively. From the cross-sectional SEM images in Figs. 2(d)–2(f), the thicknesses of the Ti/DLC, TiC_x/DLC, and Ti–TiC_x/DLC were 1.45, 1.30, and 1.45 μm, respectively. Additionally, the coatings closely adhered to the substrates and displayed a periodic multilayer structure, in which the DLC layer was compact and uniform, and the interlayer revealed different columnar growth characteristics, resulting in the roughness decreasing in the order of Ti/DLC, Ti–TiC_x/DLC, and TiC_x/DLC coatings.

Figure S2 in the ESM and Table 1 show the Raman spectra of the Ti/DLC, TiC_x/DLC, and Ti–TiC_x/DLC coatings. The fitted D peak position, G peak position, and I_D/I_G ratio remained stable at approximately 1,548 ± 3 cm^{-1}, 1,548 ± 3 cm^{-1}, and 0.59 ± 0.04, respectively, which revealed the same atomic bond structure of the top DLC layer [35, 36].

Figure 3 shows the cross-sectional TEM images and corresponding selected area electron diffraction (SAED) patterns of the Ti/DLC, TiC_x/DLC, and

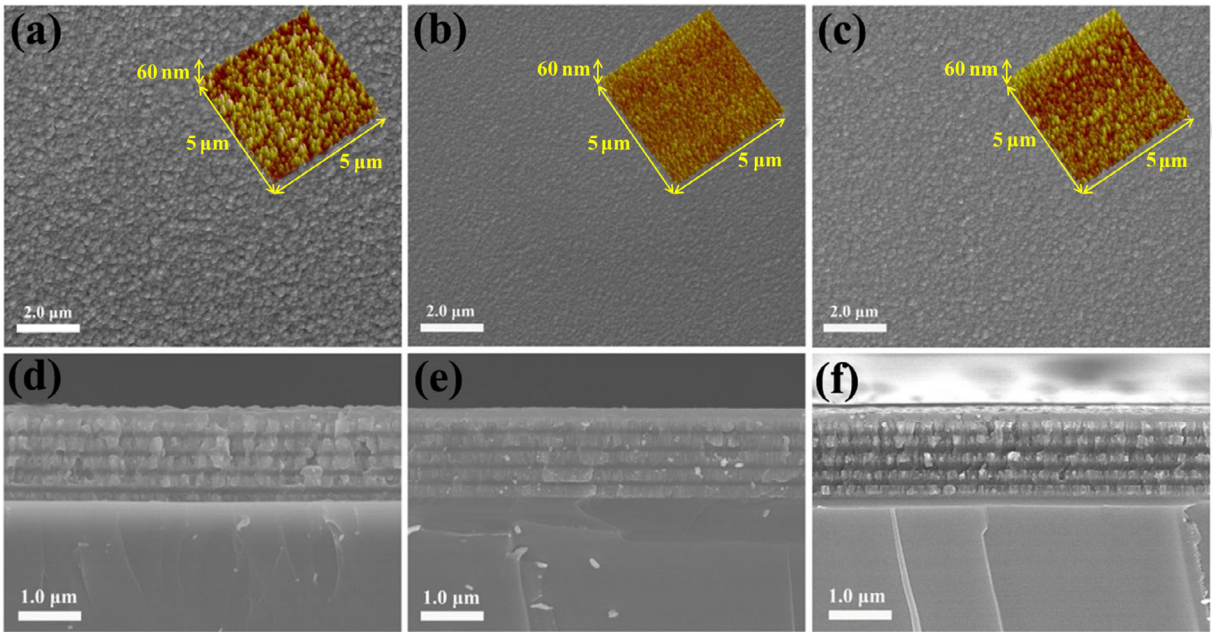

Fig. 2 Surface and cross-sectional SEM images of the (a, d) Ti/DLC, (b, e) TiC_x/DLC, and (c, f) Ti−TiC_x/DLC multilayered coatings; insets in (a)–(c) are the AFM surface topographies of the multilayered coatings.

Table 1 Raman fitting results of the multilayered coatings.

Sample	D peak position (cm^{-1})	G peak position (cm^{-1})	I_D/I_G
Ti/DLC	1,367.64	1,545.84	0.56
TiC_x/DLC	1,376.55	1,550.54	0.63
Ti−TiC_x/DLC	1,372.40	1,548.33	0.59

Ti–TiC_x/DLC coatings. As shown in Figs. 3(a)–3(d), the *c* lattice parameter deduced from the HRTEM image indicated that the Ti layer in Ti/DLC coating was a typical α-Ti (101) phase structure with columnar growth. In addition, a TiC (111) layer with thickness of 3–5 nm emerged at the interface between the α-Ti layer and the DLC layer. In Fig. 3(e), the multilayer structure similar to Fig. 3(a) can be observed, the corresponding HRTEM images presented the amorphous characteristics of DLC layer (Fig. 3(f)), the morphology of the interface between TiC_x and DLC (Fig. 3(g)), and the distribution of the nanocrystals in the TiC_x layer (Fig. 3(h)). The TiC (200) nanocrystals (marked by yellow circles in Figs. 3(g) and 3(h)) did not show significant columnar growth characteristics, as confirmed by the inverse Fourier transform in HRTEM and SAED. The different columnar growth characteristics of Ti and TiC_x layers can lead to smoother interface and surface features in the TiC_x/DLC, compared with the Ti/DLC coating. And in the Ti–TiC_x/DLC coating, since the Ti layer was not fully grown because of its short growth time, the morphological features of Ti–TiC_x layer were rather intermediary between Ti and TiC_x layers, as shown in Figs. 3(i) and 3(j). Therefore, the roughness of the coating was between those of the Ti/DLC and the TiC_x/DLC; this is consistent with the AFM results.

3.2 Mechanical properties

The nanohardness (*H*) and elastic modulus (*E*) of the coatings were measured via the nanoindentation method, as shown in Figs. S3 and S4 in the ESM and Table 2. Notably, H/E and H^3/E^2 were the main parameters reflecting their elastic-plastic deformation properties, which are closely related to the fracture toughness and wear resistance [37–43]. Generally, the higher the values of H/E and H^3/E^2, the higher are the fracture toughness and wear resistance of the materials [37–44]. As listed in Table 2, the H/E and H^3/E^2 values of the Ti/DLC, TiC_x/DLC, and Ti–TiC_x/DLC were 0.055/0.022, 0.101/0.157, and 0.079/0.072 GPa, respectively. Therefore, the TiC_x/DLC should obtain the highest fracture toughness and wear resistance among the coatings.

Furthermore, Vickers indentations were conducted to compare their plane strain fracture toughness (K_{IC})

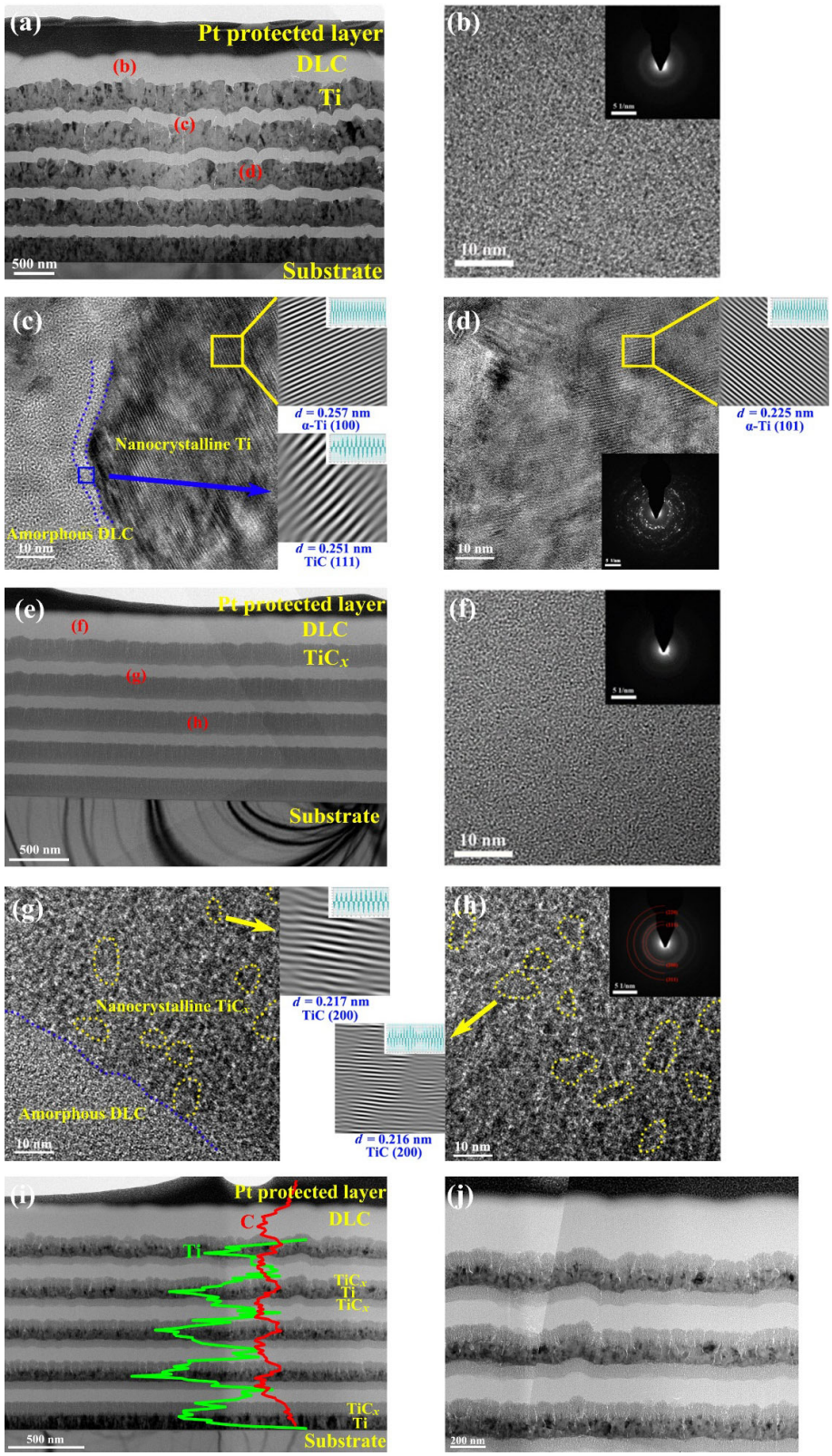

Fig. 3 (a) Cross-sectional TEM images of Ti/DLC coating, and corresponding HRTEM/SAED of various layers in Ti/DLC: (b) DLC layer, (c) interface between Ti and DLC, (d) Ti layer; (e) cross-sectional TEM images of TiC_x/DLC coating, and corresponding HRTEM/SAED of various layers in TiC_x/DLC: (f) DLC layer, (g) interface between TiC_x and DLC, (h) Ti layer; (i) cross-sectional TEM images of Ti−TiC_x/DLC coatings at low magnification and (j) high magnification.

Table 2 Summary of the mechanical properties of the coatings.

Sample	H (GPa)	E (GPa)	H/E	H^3/E^2 (GPa)	K_{IC} (MPa·m$^{1/2}$)
Ti/DLC	7.17	129.64	0.055	0.022	1.43
TiC$_x$/DLC	15.31	151.08	0.101	0.157	1.22
Ti−TiC$_x$/DLC	11.57	146.71	0.079	0.072	1.48

directly [45–47]. Figure S5 in the ESM shows SEM images of micro Vickers indentations with a normal load of 4.9 N, both in the radial and axial directions. The K_{IC} values of the Ti/DLC, TiC$_x$/DLC, and Ti–TiC$_x$/DLC based on the following indentation K_{IC} model equation were 1.43, 1.22, 1.48 MPa·m$^{1/2}$, respectively,

$$K_{IC} = \delta\left(\frac{E}{H}\right)^{1/2}\left(\frac{F}{c^{3/2}}\right) \quad (1)$$

where δ is the empirical constant, F is the indentation load, and C is the crack length [48, 49]. Evidently, the TiC$_x$/DLC exhibited the lowest K_{IC}, which was approximately 14.7% and 17.6% lower than those of the Ti/DLC and the Ti–TiC$_x$/DLC, respectively; this was contrary to the nanoindentation results. This is because the various interfaces within the coating may inhibit and hinder the growth and expansion of microcracks [37].

The aforedescribed mechanical properties test indicated that the Ti/DLC had the lowest hardness of 7.17 GPa and a high fracture toughness. The TiC$_x$/DLC exhibited the highest hardness of 15.13 GPa and the lowest fracture toughness of 1.22 MPa·m$^{1/2}$, whereas the Ti–TiC$_x$/DLC exhibited moderate hardness and the highest fracture toughness of 1.48 MPa·m$^{1/2}$.

3.3 Tribocorrosion

First, the short-term tribocorrosion properties of the coatings were evaluated, and the continuous tribocorrosion test was conducted in a 3.5 wt% NaCl solution with normal load of 5 N for 1 h.

Figure 4 shows the evolution of the OCP relative to the saturated calomel electrode (SCE) and COF

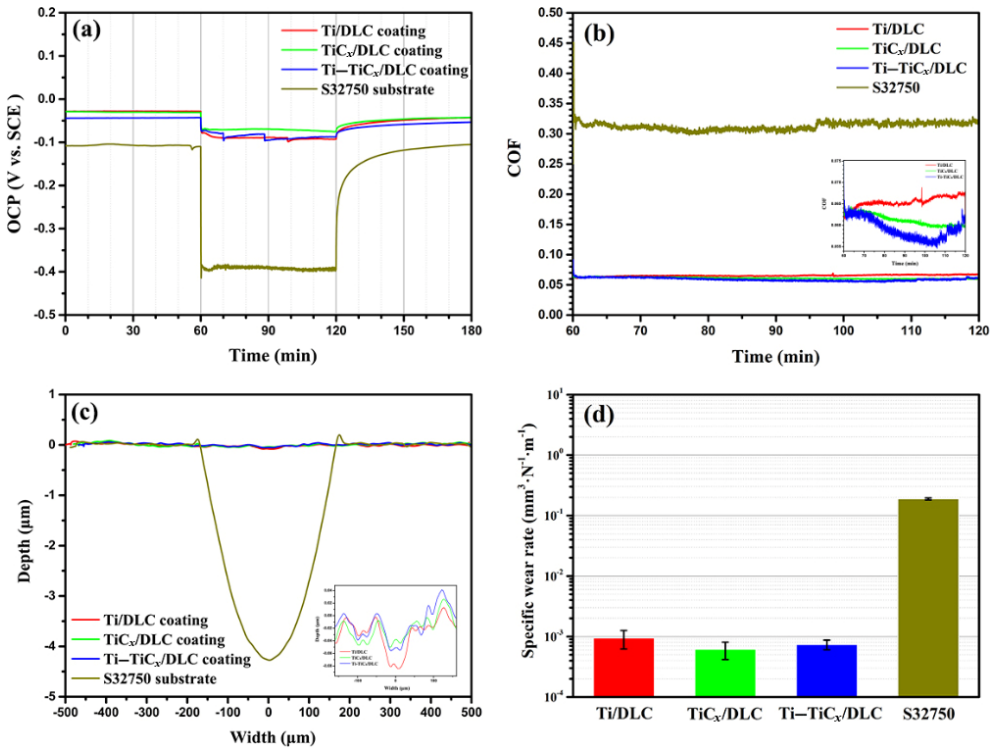

Fig. 4 Evolution of (a) OCP and (b) COF with time, and corresponding (c) cross-sectional profiles and (d) specific wear rates for the coated and bare samples in the short-term tribocorrosion test.

with test time, and the corresponding cross-sectional profiles and specific wear rate for the coated and bare S32750. In general, the OCP evolution was closely related to the electrochemical status of the electrode surface under tribocorrosion condition, indicating the surface electrochemical reactivity [50, 51]. As shown in Fig. 4(a), the pristine S32750 stainless steel displayed a sharp negative shift in the OCP curve at the beginning of tribocorrosion test. Since the passive film could be formed due to strong anodic polarization under oxidation conditions, the corrosion was then suppressed. With the consumption and removal of passive film from the contact surface during friction, the mechanical damage occurred for the sliding counterparts [50, 52]. Considering the coated samples behaved the larger OCP values than that of S32750, the higher chemical inertness and better corrosion resistance in thermodynamics could be expected. Moreover, these OCP showed the excellent stabilization despite of a slight potential drop during all tribocorrosion test, implying the higher capacity to resist mechanical wear in corrosive environments. In addition, the COF of the S32750 decreased significantly from ~0.31 to ~0.06 after coating with the multilayer coatings, as shown in Fig. 4(b), which justified their good lubrication properties. That is because top-layer DLC coating can significantly decrease the COF in short-term test [14]. Compared with the bare S32750, as shown in Fig. 4(c), the wear tracks of the coatings were difficult to observe, which indicates that the three coatings can greatly improve the wear resistance of the S32750 substrates by reducing the wear rate by more than two orders of magnitude, as shown in Fig. 4(d).

The wear track morphologies of the bare substrate and the coated samples after the tribocorrosion test are shown in Fig. 5. As displayed in Figs. 5(a) and 5(b), various plowed grooves were observed in the wear track of the S32750 substrate, which indicates the abrasive wear process. However, for the coated sample, there were only slight scratches and wear tracks on the surface, as shown in Figs. 5(c)–5(h), demonstrating the characteristics of typical uniform wear. The wear tracks of the Ti/DLC coating were evident owing to their low hardness, whereas both the TiC_x/DLC and Ti–TiC_x/DLC multilayered coatings presented the extremely narrow wear tracks, which was almost invisible for TiC_x/DLC case.

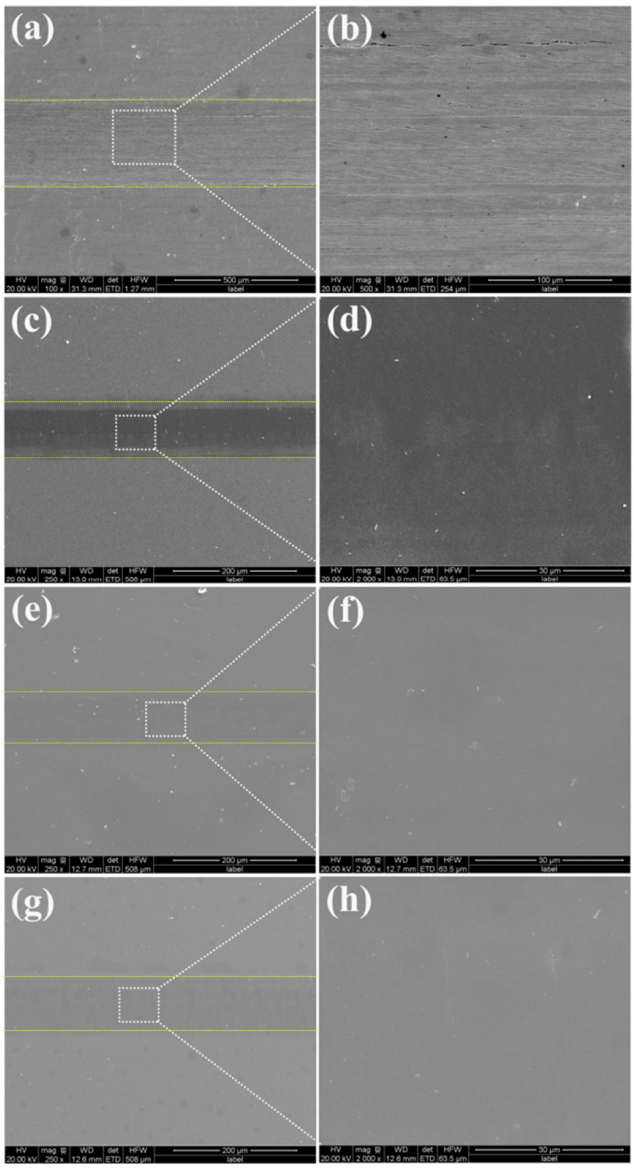

Fig. 5 SEM morphologies of wear track of the (a, b) S32750 substrate, (c, d) Ti/DLC, (e, f) TiC_x/DLC, and (g, h) Ti–TiC_x/DLC after the short-term tribocorrosion test.

To evaluate their long-term tribocorrosion properties and the failure mechanism, continuous tribocorrosion tests in a 3.5 wt% NaCl with normal load of 5 N for 12 h were conducted, as shown in Fig. 6. Figure 6(a) shows the OCP changes for various coatings. Different with the stabilized OCP for Ti–TiC_x/DLC coating during the test process, both the Ti/DLC and TiC_x/DLC coatings exhibited the slow decline after the tribocorrosion running beyond of 9 h and 3 h, respectively. Considering the aggravated corrosive attack and mechanical wear, these changes might be arisen from the extended propagations in micropores

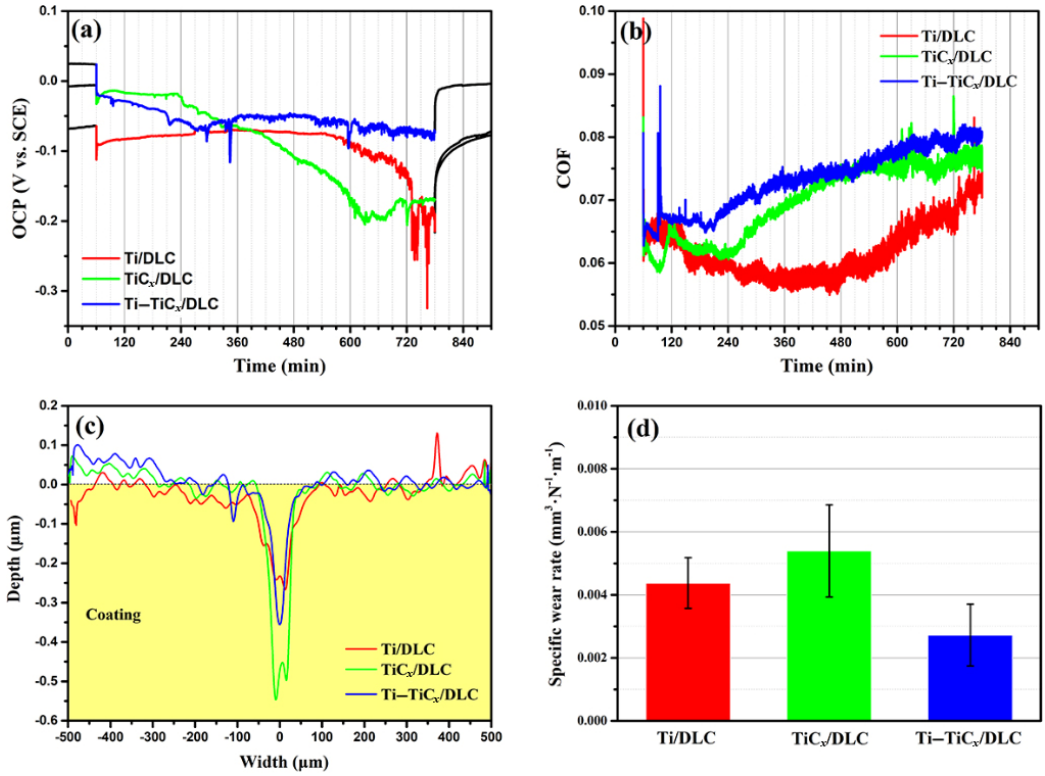

Fig. 6 Evolution of (a) OCP and (b) COF with time, and corresponding (c) cross-sectional profiles and (d) specific wear rates for the coated samples in the tribocorrosion test in a 3.5 wt% NaCl with normal load of 5 N for 12 h.

or microcracks of simple layered coatings [52, 53]. In addition, the COF of the coatings was maintained between 0.06–0.08 during the entire process. From the cross-sectional wear tracks in Fig. 6(b), the maximum depth of the wear tracks was less than 0.6 μm; that is, no coatings were worn out in the test. In addition, the Ti–TiC$_x$/DLC exhibited the smallest specific wear rate of approximately 9.82×10^{-4} mm^3·N^{-1}·m^{-1}, as displayed in Fig. 6(c), whereas the TiC$_x$/DLC exhibited the highest specific wear rate of approximately 5.40×10^{-3} mm^3·N^{-1}·m^{-1}.

The wear track morphologies of the coated samples after 12 h of the tribocorrosion test are shown in Fig. 7. Both local delamination and peeling were observed in the wear tracks of the Ti/DLC and the TiC$_x$/DLC coatings, which can provide a channel for aggressive anions and accelerate dissolution in the 3.5 wt% NaCl [54]. However, as shown in Figs. 7(e) and 7(f), the Ti–TiC$_x$/DLC coatings demonstrated the characteristics of uniform wear and no significant damage was observed.

Comparing the short-term (1 h) and long-term (12 h) tribocorrosion tests under 5 N, the Ti–TiC$_x$/DLC coating showed the best performance owing to its best comprehensive mechanical properties (moderate hardness and high fracture toughness). Moreover, the Ti–TiC$_x$/DLC coating displayed a greater advantage over the other two coatings when the normal load was further increased to 10 N in the 12 h tribocorrosion test, as shown in Figs. S6 and S7 in the ESM.

Therefore, the Ti–TiC$_x$/DLC coating was selected for further tribocorrosion tests under two harsher conditions, that is, one under 5 N with a prolonged time of 24 h and the other was under an increased normal load of 20 N for 12 h. For the 24 h test under 5 N, the COF was maintained constant at approximately 0.06 during the entire test, as shown in Fig. 8(a). Similarly, the OCP decreased from –0.04 to –0.15 V during the first sliding of 5 h, and it then remained constant situation. As shown in Fig. 8(b), the depth of the wear tracks was approximately 1.2 μm, and slight local peeling and some plowed grooves were observed at the wear tracks. This indicated that the Ti–TiC$_x$/DLC could function properly for more than 24 h (sliding

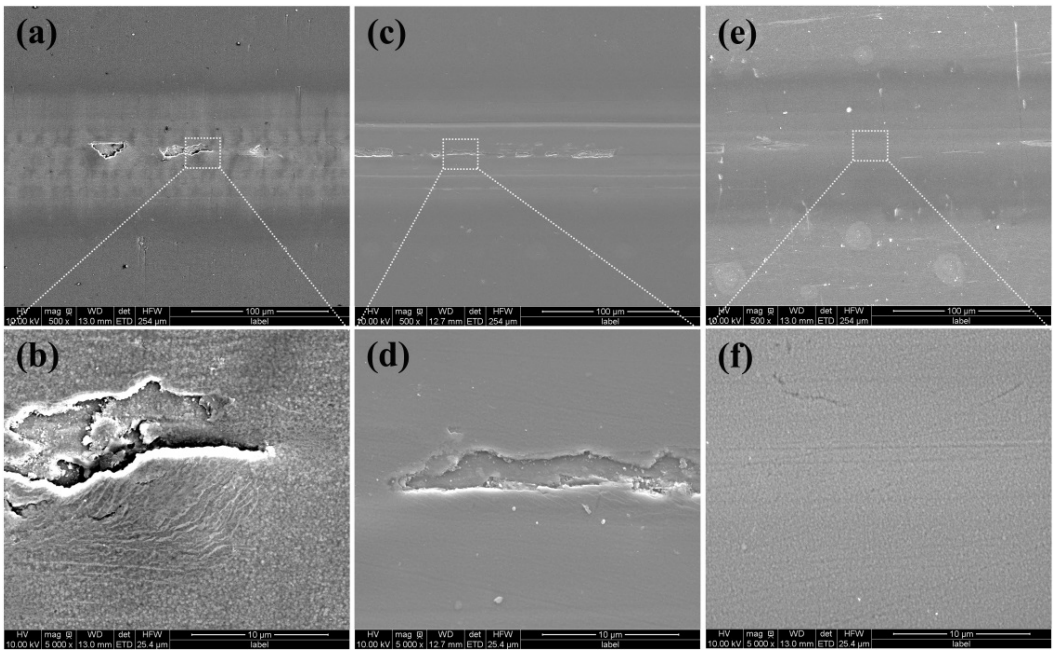

Fig. 7 SEM morphologies of the wear tracks of the (a, b) Ti/DLC, (c, d) TiC_x/DLC, and (e, f) Ti–TiC_x/DLC after a 12 h tribocorrosion test.

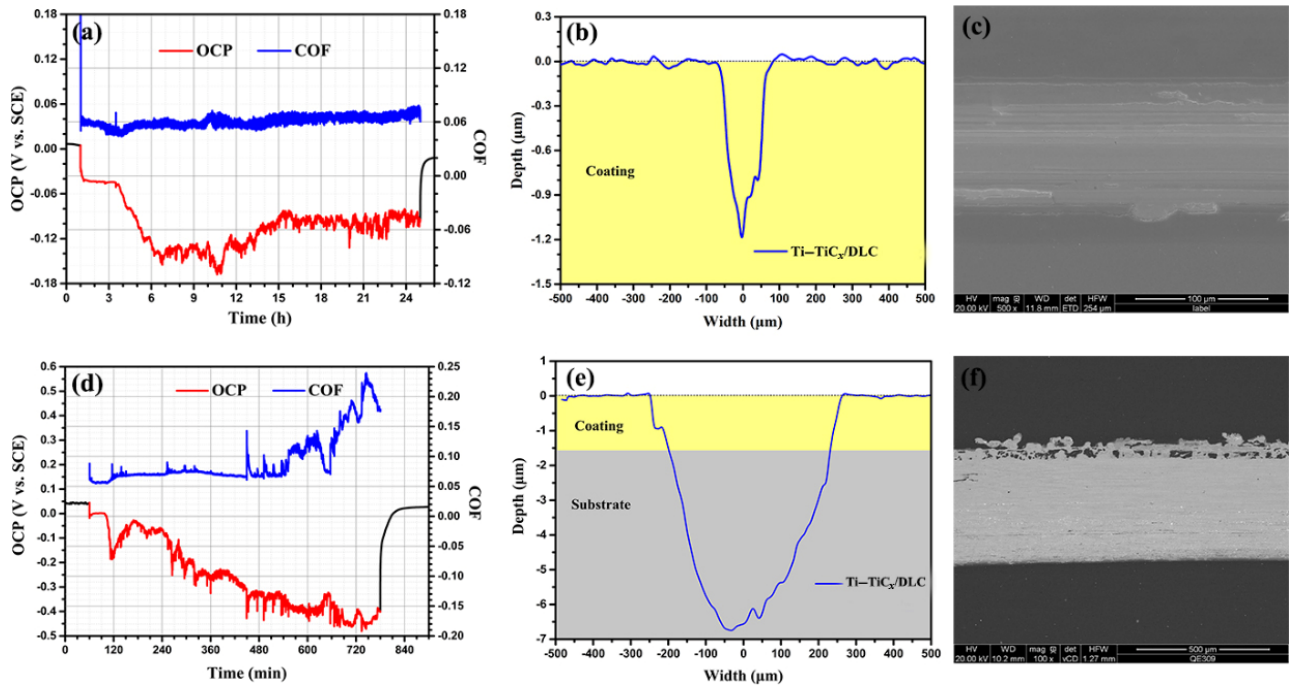

Fig. 8 (a) Evolution of OCP and COF with time, (b) corresponding cross-section profiles, and (c) SEM morphologies of wear tracks of the Ti–TiC_x/DLC after 24 h of tribocorrosion test with a normal load of 5 N; (d) evolution of OCP and COF with time, (e) corresponding cross-sectional profiles, and (f) SEM morphologies of wear tracks of the Ti–TiC_x/DLC after 12 h of tribocorrosion test with a normal load of 20 N.

distance of approximately 1,728 m). However, under the normal load of 20 N, the Ti–TiC_x/DLC was completely worn out after 12 h and the substrate was completely exposed, as shown in Figs. 8(d)–8(f).

3.4 Failure tolerance analysis

During the tribocorrosion test, the damage tolerance of the carbon-based coatings was observed. As shown

in Fig. S6(a) in the ESM and Fig. 8(d), the COFs of all the coatings were lower than those of the substrates although the coatings were worn out, that is, they can still represent wear resistances and lubrication properties.

To reveal the relevant mechanism of damage tolerance, the wear track of the Ti–TiC$_x$/DLC under 20 N for 12 h was investigated.

According to the SEM and EDS analyses, some oxygen-containing substances were detected in the area where the Ti–TiC$_x$/DLC was completely worn out. In addition, Raman tests showed that amorphous carbon existed on the surface of wear tracks in the different areas of interest, indicated by the presence of D and G peaks at approximately 1,350 cm^{-1} and 1,580 cm^{-1}, respectively, as shown in Fig. 9. As shown in Fig. 9(b), no amorphous carbon was detected in the middle area one on the wear track, and the I_D/I_G in area 2 was 0.83, higher than that of area 3. This suggests that the graphitization of amorphous carbon, which is crucial for decreasing the COF and wear volume under dry sliding tests; however, these amorphous carbon debris were difficult to stabilize on the surface because of scouring in the solution environment [11, 55].

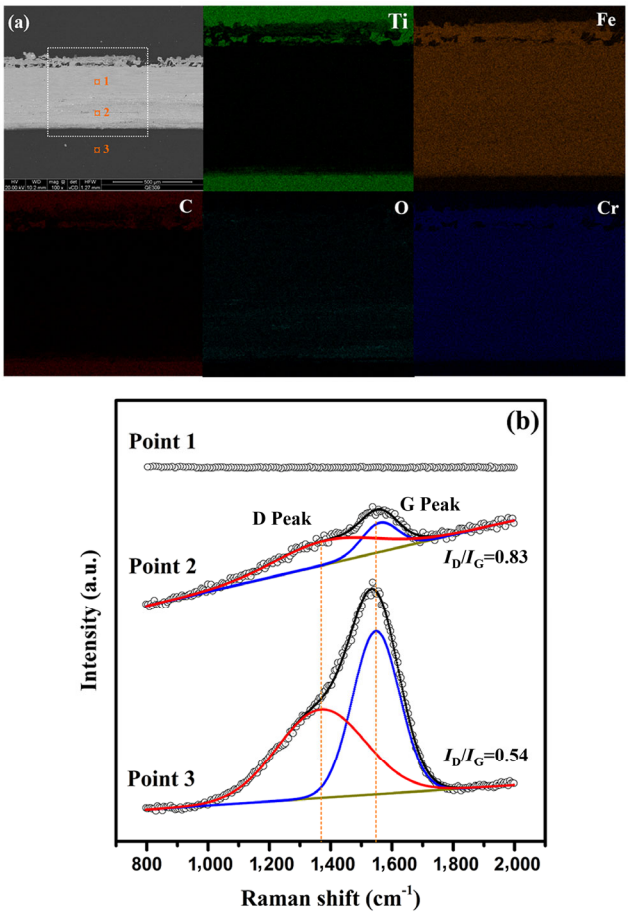

Fig. 9 (a) SEM micrographs and EDS analysis of wear tracks of the Ti–TiC$_x$/DLC after 12 h of tribocorrosion test with normal load of 20 N; (b) Raman spectra of the points marked in (a).

The cross-sectional TEM images, EDS mapping analysis, and corresponding SAED patterns were used to investigate the wear tracks, as shown in Fig. 10. The surface of wear tracks was rich in Fe, O, and C, as shown in Fig. 10(b). Fe$_x$O$_y$ nanocrystals with sizes of 3–5 nm were distributed in the amorphous carbon matrix, as displayed in Fig. 10(d), and the Fe$_x$O$_y$ particles could form a lubrication layer in the wear tracks [56].

From the above-mentioned analysis, the damage tolerance of the carbon-based coating can be explained as follows. In the short-term tribocorrosion test, the carbon-based coatings were not worn out. Therefore, they improved the anti-tribocorrosion properties of the metallic substrate, with increasing test time or load, local peeling, plowed grooves, and complete spalling of the carbon-based coating can occur. Meanwhile, as shown in Fig. 11, the sliding interface

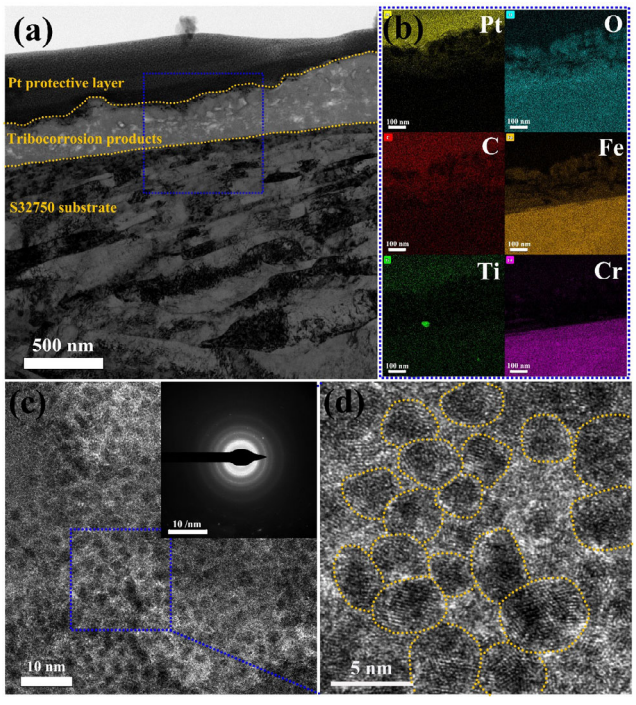

Fig. 10 (a) The cross-sectional TEM images, (b) EDS mapping analysis, (c, d) corresponding SAED, and HRTEM images of wear tracks of the Ti–TiC$_x$/DLC coatings.

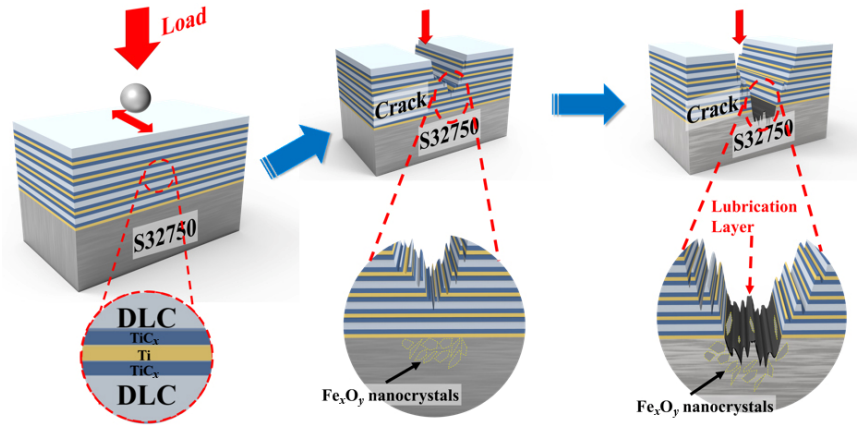

Fig. 11 Failure tolerance in long-term tribocorrosion.

indicated the graphitization of amorphous carbon and the formation of Fe_xO_y particles, which then adhered on the wear tracks to favor a stable tribofilm. As a result, the better wear resistances and lubrication was obtained during the long-term tribocorrosion tests.

4 Conclusions

Three carbon-based multilayered coatings were prepared using a hybrid system that combines LIS and DCMS in order to provide better tribocorrosion protection of the S32750 stainless steel in the marine environment. Additionally, their short-term and long-term tribocorrosion behaviors were studied, and the main conclusions are summarized as follows:

(1) For the short-term (1 h) tribocorrosion tests under 5 N, all the coatings reduced the wear rate of the S32750 substrates by more than two orders of magnitude, and the TiC_x/DLC exhibited the lowest wear rate due to its high hardness.

(2) During the long-term (12 h) tribocorrosion tests under 5 N and 10 N load, the TiC_x/DLC exhibited the worst wear resistance owing to the low fracture toughness, while the Ti–TiC_x/DLC multilayered coating with excellent fracture toughness together with high hardness displayed the highest wear resistance. It thus could be said that the fatigue resistance of the coatings played the key factor to dominate the tribological behavior for long-term tribocorrosion test. The useful lifetime of the Ti–TiC_x/DLC coating under 5 N was more than 24 h, with a sliding distance of approximately 1,728 m; however, it was completely worn out after 12 h under 20 N.

(3) During the tribocorrosion tests, the stabilization of formed tribofilm in sliding interface, consisting graphitized amorphous carbon and Fe_xO_y particles, also enabled the good damage tolerance for the carbon- based coating.

Acknowledgements

This work was supported by the National Natural Science Foundation of China (Nos. 52025014 and 51801226), A-class pilot of the Chinese Academy of Sciences (No. XDA22010303), K.C. Wong Education Foundation (No. GJTD-2019-13), CAS-NST Joint Research Project (No. 174433KYSB20200021), and CAS Interdisciplinary Innovation Team (No. 292020000008).

Electronic Supplementary Material: Supplementary Material is available in the online version of this article at https://doi.org/10.1007/s40544-021-0559-4.

References

[1] Wang Y X, Wang N. The role of the marine industry in China's national economy: An input-output analysis. *Mar Policy* **99**: 42–49 (2019)

[2] Wood R J K. Marine wear and tribocorrosion. *Wear* **376–377**: 893–910 (2017)

[3] Wu Z W, Zhou F, Ma Q, Wang Q Z, Zhou Z F, Li L K-Y. Tribological and electrochemical properties of Cr–Si–C–N coatings in artificial seawater. *RSC Adv* **6**(80): 76724–76735 (2016)

[4] Liu Z, Chu Z H, Chen X G, Dong Y C, Yang Y, Li Y Z, Yan D R. Electrochemical impedance studies on tribocorrosion behavior of plasma-sprayed Al_2O_3 coatings. *J Therm Spray Technol* **24**(5): 878–884 (2015)

[5] Totolin V, Pejaković V, Csanyi T, Hekele O, Huber M, Rodríguez Ripoll M. Surface engineering of Ti_6Al_4V surfaces for enhanced tribocorrosion performance in artificial seawater. *Mater Des* **104**: 10–18 (2016)

[6] Sui X D, Xu R N, Liu J, Zhang S T, Wu Y, Yang J, Hao J Y. Tailoring the tribocorrosion and antifouling performance of (Cr, Cu)-GLC coatings for marine application. *ACS Appl Mater Interfaces* **10**(42): 36531–36539 (2018)

[7] Azzi M, Paquette M, Szpunar J A, Klemberg-Sapieha J E, Martinu L. Tribocorrosion behaviour of DLC-coated 316L stainless steel. *Wear* **267**(5–8): 860–866 (2009)

[8] Arslan E, Totik Y, Efeoglu I. The investigation of the tribocorrosion properties of DLC coatings deposited on Ti_6Al_4V alloys by CFUBMS. *Prog Org Coat* **74**(4): 768–771 (2012)

[9] Kim J G, Lee K R, Yang S J. Wear-corrosion performance of Si-DLC coatings on Ti-6Al-4V substrate. *J Biomed Mater Res A* **86**(1): 41–47 (2008)

[10] Ye Y W, Wang Y X, Ma X L, Zhang D W, Wang L P, Li X G. Tribocorrosion behaviors of multilayer PVD DLC coated 304L stainless steel in seawater. *Diam Relat Mater* **79**: 70–78 (2017)

[11] Sun L, Zuo X, Guo P, Li X, Ke P, Wang A. Role of deposition temperature on the mechanical and tribological properties of Cu and Cr co-doped diamond-like carbon films. *Thin Solid Films* **678**: 16–25 (2019)

[12] Li X, Li L, Zhang D, Wang A. Ab initio study of interfacial structure transformation of amorphous carbon catalyzed by Ti, Cr, and W transition layers. *ACS Appl Mater Interfaces* **9**(47): 41115–41119 (2017)

[13] Fu Y Q, Loh N L, Wei J, Yan B B, Hing P. Friction and wear behaviour of carbon nitride films deposited on plasma nitrided Ti-6Al-4V. *Wear* **237**(1): 12–19 (2000)

[14] Meletis E I, Erdemir A, Fenske G R. Tribological characteristics of DLC films and duplex plasma nitriding/DLC coating treatments. *Surf Coat Technol* **73**(1–2): 39–45 (1995)

[15] Zhang M, Wu B, Lin G Q, Shao Z G, Hou M, Yi B L. Arc ion plated Cr/CrN/Cr multilayers on 316L stainless steel as bipolar plates for polymer electrolyte membrane fuel cells. *J Power Sources* **196**: 3249–3254 (2011)

[16] Bai W Q, Li L L, Xie Y J, Liu D G, Wang X L, Jin G, Tu J P. Corrosion and tribocorrosion performance of M (M=Ta, Ti) doped amorphous carbon multilayers in Hank's solution. *Surf Coat Tech* **305**: 11–22 (2016)

[17] He G Y, Zhu X D, He W F, Chai Y. GLC coating improving the wear resistance of aeroengine bearings in insufficient lubrication. In *2013 International Conference on Process Equipment, Mechatronics Engineering and Material Science*, Trans Tech Publications Ltd, Durnten-Zurich, 2013: 48.

[18] Zhang R H, Wang L P. Synergistic improving of tribological properties of amorphous carbon film enhanced by F-Si-doped multilayer structure under corrosive environment. *Surf Coat Technol* **276**: 626–635 (2015)

[19] Shan L, Wang Y X, Zhang Y R, Zhang Q, Xue Q J. Tribocorrosion behaviors of PVD CrN coated stainless steel in seawater. *Wear* **362–363**: 97–104 (2016)

[20] Ye Y W, Wang Y X, Wang C T, Li J L, Yao Y R. An analysis on tribological performance of CrCN coatings with different carbon contents in seawater. *Tribol Int* **91**: 131–139 (2015)

[21] Mubarok F, Espallargas N. Tribological behaviour of thermally sprayed silicon carbide coatings. *Tribol Int* **85**: 56–65 (2015)

[22] Armada S, Tilset B G, Pilz M, Liltvedt R, Bratland H, Espallargas N. Sealing HVOF thermally sprayed WC-CoCr coatings by sol-gel methods. *J Therm Spray Technol* **20**(4): 918–926 (2011)

[23] Liu X, Zhao X Q, An Y L, Hou G L, Li S J, Deng W, Zhou H D, Chen J M. Effects of loads on corrosion-wear synergism of NiCoCrAlYTa coating in artificial seawater. *Tribol Int* **118**: 421–431 (2018)

[24] Wang Y, Li J L, Dang C Q, Wang Y X, Zhu Y J. Influence of carbon contents on the structure and tribocorrosion properties of TiSiCN coatings on Ti_6Al_4V. *Tribol Int* **109**: 285–296 (2017)

[25] Sun S Q, Ye Y W, Wang Y X, Liu M Q, Liu X, Li J L, Wang L P. Structure and tribological performances of CrAlSiN coatings with different Si percentages in seawater. *Tribol Int* **115**: 591–599 (2017)

[26] Li J L, Zhong H S, Wang Y X. Dynamic tribochemical behavior of TiN/TiCN coated Ti_6Al_4V in artificial seawater. *RSC Adv* **6**(107): 105854–105861 (2016)

[27] Li L, Liu LL, Li X, Guo P, Ke P, Wang A. Enhanced tribocorrosion performance of Cr/GLC multilayered films for marine protective application. *ACS Appl Mater Interfaces* **10**(15): 13187–13198 (2018)

[27] López-Ortega A, Arana J L, Rodríguez E, Bayón R. Corrosion, wear and tribocorrosion performance of a thermally sprayed aluminum coating modified by plasma electrolytic oxidation technique for offshore submerged components protection. *Corros Sci* **143**: 258–280 (2018)

[29] Pu J B, Wang J J, He D Q, Wan S H. Corrosion and tribocorrosion behaviour of super-thick diamond-like carbon films deposited on stainless steel in NaCl solution. *Surf Interface Anal* **48**(6): 360–367 (2016)

[30] von der Ohe C B, Johnsen R, Espallargas N. Multi-degradation behavior of austenitic and super duplex stainless steel - The effect of 4-point static and cyclic bending applied to a simulated seawater tribocorrosion system. *Wear* **288**: 39–53 (2012)

[31] Silva R C C, Nogueira R P, Bastos I N. Tribocorrosion of UNS S32750 in chloride medium: Effect of the load level. *Electrochimica Acta* **56**(24): 8839–8845 (2011)

[32] Dwivedi N, Kumar S, Malik H K. Nanostructured titanium/diamond-like carbon multilayer films: Deposition, characterization, and applications. *ACS Appl Mater Interfaces* **3**(11): 4268–4278 (2011)

[33] Bulíř J, Novotný M, Jelínek M, Kocourek T, Studnička V. Plasma study and deposition of DLC/TiC/Ti multilayer structures using technique combining pulsed laser deposition and magnetron sputtering. *Surf Coat Technol* **200**(1–4): 708–711 (2005)

[34] Cheng F, Wu F J, Liu L L, Yang S F, Ji W X. Investigation on cavitation erosion of diamond-like carbon films with heterogeneous multilayer structure. *Surf Coat Technol* **405**: 126682 (2021)

[35] Chen X C, Peng Z J, Yu X, Fu Z Q, Yue W, Wang C B. Microstructure and tribological performance of self-lubricating diamond/tetrahedral amorphous carbon composite film. *Appl Surf Sci* **257**(8): 3180–3186 (2011)

[36] Ferrari A C, Robertson J. Interpretation of Raman spectra of disordered and amorphous carbon. *Phys Rev B* **61**(20): 14095–14107 (2000)

[37] Chen X J, Du Y, Chung Y W. Commentary on using H/E and H^3/E^2 as proxies for fracture toughness of hard coatings. *Thin Solid Films* **688**: 137265 (2019)

[38] Zhang S D, Yan M F, Yang Y, Zhang Y X, Yan F Y, Li H T. Excellent mechanical, tribological and anti-corrosive performance of novel Ti-DLC nanocomposite thin films prepared via magnetron sputtering method. *Carbon* **151**: 136–147 (2019)

[39] Ren P, Wen M, Zhang K, Du S X, Zhang Y D, Chen J H, Zheng W T. Self-assembly of TaC@Ta core-shell-like nanocomposite film via solid-state dewetting: Toward superior wear and corrosion resistance. *Acta Mater* **160**: 72–84 (2018)

[40] Li L L, Bai W Q, Wang X L, Gu C D, Jin G, Tu J P. Mechanical properties and *in vitro* and *in vivo* biocompatibility of a-C/a-C: Ti nanomultilayer films on Ti_6Al_4V alloy as medical implants. *ACS Appl Mater Interfaces* **9**(19): 15933–15942 (2017)

[41] Ren P, Zhang K, He X, Du S X, Yang X Y, An T, Wen M, Zheng W T. Toughness enhancement and tribochemistry of the Nb-Ag-N films actuated by solute Ag. *Acta Mater* **137**: 1–11 (2017)

[42] Lin J L, Wei R H, Bitsis D C, Lee P M. Development and evaluation of low friction TiSiCN nanocomposite coatings for piston ring applications. *Surf Coat Technol* **298**: 121–131 (2016)

[43] Yang Y, Yan M F, Zhang Y X, Li D Y, Zhang C S, Zhu Y D, Wang Y X. Catalytic growth of diamond-like carbon on Fe3C-containing carburized layer through a single-step plasma-assisted carburizing process. *Carbon* **122**: 1–8 (2017)

[44] Mockute A, Palisaitis J, Alling B, Berastegui P, Broitman E, Näslund L Å, Nedfors N, Lu J, Jensen J, Hultman L, *et al*. Age hardening in $(Ti_{1-x}Al_x)B_2 + \Delta$ thin films. *Scr Mater* **127**: 122–126 (2017)

[45] Liu J Z, Zuo X, Wang Z Y, Wang L, Wu X C, Ke P L, Wang A Y. Fabrication and mechanical properties of high purity of Cr_2AlC coatings by adjustable Al contents. *J Alloys Compd* **753**: 11–17 (2018)

[46] Song K, Xu Y H, Zhao N N, Zhong L S, Shang Z, Shen L L, Wang J. Evaluation of fracture toughness of tantalum carbide ceramic layer: A vickers indentation method. *J Mater Eng Perform* **25**(7): 3057–3064 (2016)

[47] Oliver W C, Pharr G M. An improved technique for determining hardness and elastic modulus using load and displacement sensing indentation experiments. *J Mater Res* **7**(6): 1564–1583 (1992)

[48] Lawn B R, Evans A G, Marshall D B. Elastic/plastic indentation damage in ceramics: The Median/radial crack system. *J Am Ceram Soc* **63**(9–10): 574–581 (1980)

[49] Evans A G, Charles E A. Fracture toughness determinations by indentation. *J Am Ceram Soc* **59**(7–8): 371–372 (1976)
[50] Bayón R, Igartua A, González J J, de Gopegui U R. Influence of the carbon content on the corrosion and tribocorrosion performance of Ti-DLC coatings for biomedical alloys. *Tribol Int* **88**: 115–125 (2015)
[51] Yan Y, Neville A, Dowson D. Tribo-corrosion properties of cobalt-based medical implant alloys in simulated biological environments. *Wear* **263**(7–12): 1105–1111 (2007)
[52] Liu J, Wang X, Wu B J, Zhang T F, Leng Y X, Huang N. Tribocorrosion behavior of DLC-coated CoCrMo alloy in simulated biological environment. *Vacuum* **92**: 39–43 (2013)
[53] Manhabosco T M, Barboza A P M, Batista R J C, Neves B R A, Müller I L. Corrosion, wear and wear-corrosion behavior of graphite-like a-C: H films deposited on bare and nitrided titanium alloy. *Diam Relat Mater* **31**: 58–64 (2013)
[54] Gao S J, Dong C F, Luo H, Xiao K, Pan X M, Li X G. Scanning electrochemical microscopy study on the electrochemical behavior of CrN film formed on 304 stainless steel by magnetron sputtering. *Electrochimica Acta* **114**: 233–241 (2013)
[55] Müller I C, Sharp J, Rainforth W M, Hovsepian P, Ehiasarian A. Tribological response and characterization of Mo-W doped DLC coating. *Wear* **376–377**: 1622–1629 (2017)
[56] Yin C H, Liang Y L, Liang Y, Li W, Yang M. Formation of a self-lubricating layer by oxidation and solid-state amorphization of nano-lamellar microstructures during dry sliding wear tests. *Acta Mater* **166**: 208–220 (2019)

Hao LI. He received the B.S. degree in chemistry from Nankai University in 2015 and his M.S. degree in materials engineering from Tianjin Normal University in 2018. He is now a Ph.D. candidate at Ningbo Institute of Materials Technology and Engineering, Chinese Academy of Sciences. His research is the tribocorrosion and electrochemical behavior of amorphous carbon films.

Peng GUO. He received the Ph.D. degree from University of Chinese Academy of Sciences (CAS) in July 2015. He is currently an associate professor at Ningbo Institute of Materials Technology and Engineering (NIMTE), CAS. His research interest is the preparation and characterization of amorphous carbon films as well as application of related functional devices.

Aiying WANG. She received her Ph.D. degree from Institute of Metal Research, CAS in 2003. After graduation, she worked as a post-doctor in Korea Institute of Science and Technology and a senior researcher in Korea JNL Tech. Co. Ltd. from 2003 to 2006. Since December 2006, she has been a full professor at Ningbo Institute of Materials Technology and Engineering (NIMTE), Chinese Academy of Sciences (CAS), and the deputy director of CAS Key laboratory of Marine Materials and Related Technologies currently. Her research is mainly focused on advanced carbon films and plasma surface modification for components in harsh applications.